# Doping of Alkali, Alkaline-Earth, and Transition Metals in Covalent-Organic Frameworks for Enhancing $CO_2$ Capture by First-Principles Calculations and Molecular Simulations

**Jianhui Lan,[†] Dapeng Cao,[†,*] Wenchuan Wang,[†,*] and Berend Smit[‡]**

[†]Division of Molecular and Materials Simulation, Key Lab for Nanomaterials, Ministry of Education of China, Beijing University of Chemical Technology, Beijing 100029, People's Republic of China, and [‡]Department of Chemical Engineering and Chemistry, University of California, Berkeley, California 94720

**ABSTRACT** We use the multiscale simulation approach, which combines the first-principles calculations and grand canonical Monte Carlo simulations, to comprehensively study the doping of a series of alkali (Li, Na, and K), alkaline-earth (Be, Mg, and Ca), and transition (Sc and Ti) metals in nanoporous covalent organic frameworks (COFs), and the effects of the doped metals on $CO_2$ capture. The results indicate that, among all the metals studied, Li, Sc, and Ti can bind with COFs stably, while Be, Mg, and Ca cannot, because the binding of Be, Mg, and Ca with COFs is very weak. Furthermore, Li, Sc, and Ti can improve the uptakes of $CO_2$ in COFs significantly. However, the binding energy of a $CO_2$ molecule with Sc and Ti exceeds the lower limit of chemisorptions and, thus, suffers from the difficulty of desorption. By the comparative studies above, it is found that Li is the best surface modifier of COFs for $CO_2$ capture among all the metals studied. Therefore, we further investigate the uptakes of $CO_2$ in the Li-doped COFs. Our simulation results show that at 298 K and 1 bar, the excess $CO_2$ uptakes of the Li-doped COF-102 and COF-105 reach 409 and 344 mg/g, which are about eight and four times those in the nondoped ones, respectively. As the pressure increases to 40 bar, the $CO_2$ uptakes of the Li-doped COF-102 and COF-105 reach 1349 and 2266 mg/g at 298 K, respectively, which are among the reported highest scores to date. In summary, doping of metals in porous COFs provides an efficient approach for enhancing $CO_2$ capture.

**KEYWORDS:** covalent organic frameworks · metal-doping · $CO_2$ capture · first-principles calculations · grand canonical Monte Carlo simulation

Nowadays, the natural greenhouse effect resulting from rapid emission of greenhouse gases in the atmosphere increases significantly. Carbon dioxide is the main greenhouse gas contributing to the climate change. Therefore, $CO_2$ capture from industrial emission sources has attracted significant research interest recently.

Among present techniques for $CO_2$ capture, adsorption by using porous materials is deemed as the most promising and competitive method for $CO_2$ recovery. An ideal $CO_2$ adsorption and separation material should possess characteristics of high selectivity and high capacity. So far, a large amount of research has been focused on $CO_2$ capture in porous materials, such as covalent organic frameworks (COFs),[1,2] metal organic frameworks (MOFs),[3−16] and zeolites.[17−21] By measuring the basic data of $CO_2$ adsorption in porous materials, the intrinsic relationship between the adsorbent structure and its performance for $CO_2$ capture can thus be found out, which can provide a useful direction to the design of porous materials for $CO_2$ capture and separation.

A lot of research efforts on $CO_2$ capture in porous materials have been reported in experiment and molecular simulation recently. Millward and Yaghi measured the adsorption capacity of $CO_2$ in a series of MOFs, experimentally, and found that the $CO_2$ uptake of MOF-177 reaches about 9× the amount of $CO_2$ in a container without adsorbent at room temperature and 35 bar.[3] Bae *et al.* synthesized a mixed-ligand MOF, $Zn_2(NDC)_2(DPNI)$ [NDC = 2,6-naphthalenedicarboxylate, DPNI = *N*,*N*′-di-(4-pyridyl)-1,4,5,8-naphthalene tetracarboxydiimide], and found that this material shows a selectivity of ~30 for $CO_2$ over $CH_4$ by using the ideal adsorbed solution theory (IAST).[6] Demessence *et al.* synthesized an air- and water-stable MOF, $H_3[(Cu_4Cl)_3(BTTri)_8]$ ($H_3BTTri$ = 1,3,5-tris(1*H*-1,2,3-triazol-5-yl)benzene).[13] Their results proved that the $CO_2$ uptakes of this material reach 142.56 mg/g at 298 K and 1 bar, while exhibiting significantly higher uptakes of $CO_2$ at even lower pressure after functionalized by ethylenediamine. Britt *et al.* reported $CO_2$ capture in a competitive MOF material, Mg-MOF-74 and found that this material shows

*Address correspondence to caodp@mail.buct.edu.cn, wangwc@mail.buct.edu.cn.

Received for review May 4, 2010 and accepted June 16, 2010.

**Published online June 22, 2010.** 10.1021/nn100962r

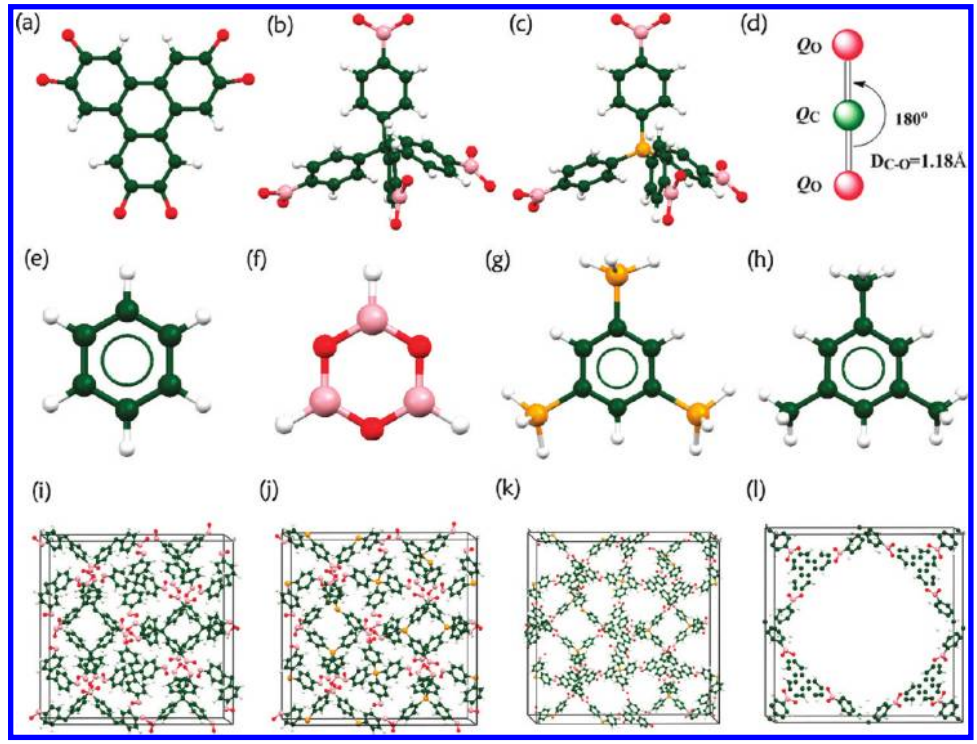


**Figure 1. (a−c) Building blocks of 3D COFs, (d) the rigid model of a $CO_2$ molecule, (e−h) selected cluster models, and (i−l) the unit cells of 3D COFs: (a) triangular hexahydroxy-triphenylene (HHTP), (b) tetrahedral tetra(4-dihydroxyborylphenyl)-methane (TBPM), (c) silane analog of TBPM (TBPS), (e) $C_6H_6$, (f) $B_3O_3H_3$, (g) $Si_3C_6H_{12}$, (h) $C_9H_{12}$, (i) COF-102, (j) COF-103, (k) COF-105, and (l) COF-108. For clarity, H atoms bonded to O in (a−c) is neglected. C, O, B, H, and Si atoms are shown as green, red, pink, white, and yellow colors, respectively.**

a dynamic capacity of 8.9 wt % and undergoes facile $CO_2$ release at a significantly lower temperature, 353 K.[14] Bourrelly *et al.* measured $CO_2$ adsorption in a MOF material, MIL-53, at 304 K and observed a distinct step in the isotherm that is characterized as a breathing behavior.[15] Llewellyn *et al.* reported that the mesoporous MIL-101(Cr) shows the $CO_2$ uptake of about 1760 mg/g at 303 K and 50 bar, exceeding all the other porous materials.[16] In addition, a series of zeolitic imidazolate frameworks (ZIFs) were synthesized recently,[19,21] and it is found that the ZIFs exhibit excellent selectivity for $CO_2$ capture due to the combined effects of the slit width of the pore apertures being similar in size to $CO_2$ (kinetic diameter, 3 Å) and the strong quadrupolar interactions of carbon with nitrogen atoms in the links. Giovanni *et al.* studied the adsorption of $CO_2$ in silica gel experimentally and reported that the $CO_2$ uptake of silica gel reaches 331 mg/g at 294 K and 45 bar.[22] Most recently, Yaghi *et al.* synthesized a family of three-dimensional (3D) covalent organic frameworks (COFs, termed COF-102, -103, -105, and -108) by self-condensation and co-condensation reactions of the rigid molecular building blocks, the tetrahedral tetra(4-dihydroxyborylphenyl)methane (TBPM), its silane analog (TBPS), and the triangular hexahydroxy-triphenylene (HHTP).[1] The experimental measurement indicates that the $CO_2$ uptake of COF-102 reaches 1200 mg/g at 298 K and 35 bar,[2] higher than MOF-5 (970 mg/g)[3] and zeolite (220−350 mg/g).[18]

In addition to experimental investigations, some theoretical studies of molecular simulations have also been performed for screening high $CO_2$ capture materials. Snurr *et al.* studied the mechanism of the steps in $CO_2$ isotherms of MOFs by molecular simulation and suggested that the attractive electrostatic interactions between $CO_2$ molecules are responsible for the unusual shape of the adsorption isotherms studied.[23] Babarao and Jiang simulated the storage of $CO_2$ in a series of MOFs at room temperature, and reported that the organic linker plays a critical role in tuning the free volume and accessible surface area and determining $CO_2$ uptakes at high pressures.[24] Ramsahye *et al.* studied the possible adsorption sites for $CO_2$ in MIL-53 (Al, Cr) and MIL-47 (V) by the density functional theory (DFT), which provides useful information for understanding the breathing behavior.[25] Besides, Torrisi *et al.* compared the intermolecular interactions between $CO_2$ and a series of functionalized aromatic molecules using the DFT method to provide directions for designing linker molecules in MOFs.[26]

It is noticed that few investigations have been focused on the influence of metal-doping on $CO_2$ capture, to the best of our knowledge, although this metal-doping strategy has been extensively studied in hydrogen storage and has been proven to be effective. These findings motivate us to look into the effect of doping of metals in COFs on $CO_2$ capture. In this work, we first study adsorption of $CO_2$ in 3D COFs by us-

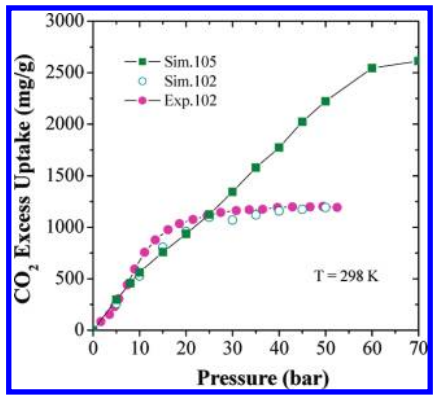


**Figure 2. Simulated excess adsorption isotherms of $CO_2$ in COFs at $T = 298$ K. For comparison, the experimental data of COF-102 are also presented.[2]**

ing a multiscale simulation method, which combines the first principles calculation and grand canonical Monte Carlo (GCMC) simulation, as reported in our previous works.[27−33] We then evaluate the impact of doping of metals in COFs on $CO_2$ capture by using the first principles calculations. The metals studied here include alkali metals (Li, Na, and K), alkaline-earth metals (Be, Mg, and Ca), and transition metals (Sc and Ti). Finally, as the best metal modifier of COFs for $CO_2$ capture, we thus investigate adsorption capacities of $CO_2$ in Li-doped COFs at room temperature by molecular simulation, aiming at verifying the doping effect.

## RESULTS AND DISCUSSION

We carried out the first-principles calculations and molecular simulations in the following aspects: (1) To simulate $CO_2$ adsorption in nondoped COFs, and compare the results to those in experiment for verifying the approach used in this work. (2) To dope alkali (Li, Na, and K), alkaline-earth (Be, Mg, and Ca), and transition metals (Sc and Ti) in COFs. (3) To investigate the doping effect on $CO_2$ adsorption. To reduce computational consuming, the commonly used cluster model method was adopted in the first-principles calculations to represent the real structure of COFs, and the representative clusters and the unit cells of 3D COFs are shown in Figure 1.

**Adsorption of $CO_2$ in Nondoped COFs.** Using the force field parameters obtained here as input (see the Supporting Information), we simulated the adsorption isotherms of $CO_2$ in COF-102 and COF-105 at room temperature as the representatives of COFs, because COF-102 and COF-103 display very close capacities for $CH_4$ and $CO_2$, while COF-105 gives very close capacities to COF-108.[2,29]

Figure 2 displays the simulated adsorption isotherms of $CO_2$ in COFs at $T = 298$ K within the pressure range up to 70 bar, where the experimental data[2] for COF-102 are also presented for calibration of our multiscale methods. It is found that our simulation results are in good agreement with experimental isotherms for COF-102, while only the simulated isotherm for COF-105 is shown in Figure 2 for lack of experimental data of COF-105.[2] Compared to COF-102, COF-105 presents much higher $CO_2$ uptakes as the pressure exceeds 20 bar due to its obviously larger pore volume and free volume[29] based on the observation that smaller pore size produces stronger framework affinity to adsorbates at low pressures, while pore volume plays a more important role at higher pressures. As the pressure equals 20 bar, the excess $CO_2$ uptake of COF-102 reaches 1076 mg/g. On the contrary, the excess $CO_2$ uptake of COF-105 increases nearly linearly up to 60 bar. At $p = 20$ and 50 bar, COF-105 presents the excess $CO_2$ uptake of 942.03 and 2224.0 mg/g, respectively, indicating that COF-105 is a very promising candidate for $CO_2$ capture and storage. As a matter of fact, the adsorption capacity of $CO_2$ in COFs is mainly dependent on the components and topologies of their frameworks. Our first principles calculations indicate that the phenyls in the TBPS or TBPM building block generate slightly weaker affinity to $CO_2$ than the heterocycle rings of $B_3O_3$ (in COF-102) and $C_2O_2B$ (in COF-105). These results can be explained as the phenyl conjugated $\pi\cdots$quadrupole of $CO_2$ interaction is weaker than the electrostatic ion (O in $B_3O_3$ or $C_2O_2B$)$\cdots$quadrupole of $CO_2$ interaction. In addition, the steric effect also makes the adsorption sites around the heterocycle rings more accessible.

**TABLE 1. Calculated Binding Energies (B.E.) of $M^+$ and a $CO_2$ Molecule**

| $M^+$ | MP2/6-311 g(d, p) (kcal/mol) | PW91/6-311 g(d,p)//B3LYP/6-31 g(d) (kcal/mol) |
|---|---|---|
| $Li^+$ | −19.752 | −21.305 |
| $Na^+$ | −12.315 | −13.874 |
| $K^+$ | −8.773 | −9.259 |
| $Be^+$ | −34.383 | −39.921 |
| $Mg^+$ | −14.751 | −17.539 |
| $Ca^+$ | −11.409 | −15.995 |
| $Sc^+$ | −34.405 | −28.035 |
| $Ti^+$ | −66.764 | −51.443 |

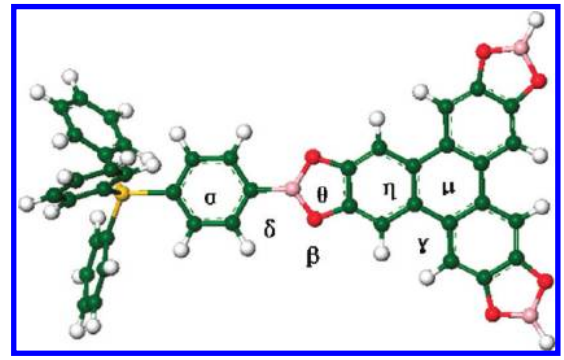


**Figure 3. Possible adsorption sites, α, β, δ, θ, η, γ, and μ, for adsorption of metals in the 3D COFs. The cluster model used here to represent the COFs is selected from COF-105, and the dangling bonds are terminated by H atoms. C, O, B, H, and Si atoms are shown as green, red, pink, white, and yellow colors, respectively.**

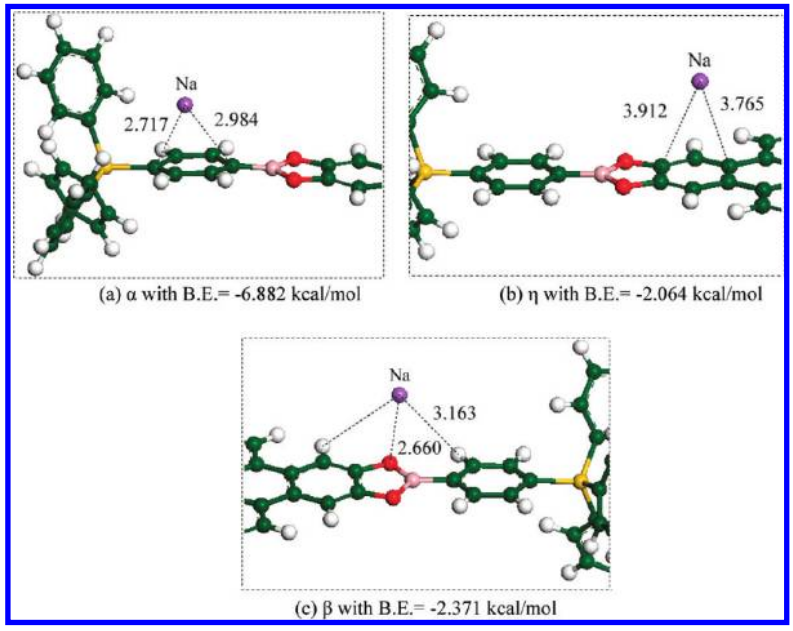


**Figure 4. Optimized adsorption sites of Na in the 3D COFs: (a) α, (b) η, and (c) β. The calculated binding energies are also shown correspondingly. The measured distances from the adsorbed Na atom to the surface are presented in Å. C, O, B, H, Si, and Na atoms are shown as green, red, pink, white, yellow, and purple colors, respectively.**

**Doping of Alkali, Alkaline-Earth, and Transition Metals in COFs.** As is well-known, doping of electropositive metals like Li to porous materials, such as COFs and MOFs, can enhance the adsorption of hydrogen significantly due to the strong affinity of positively charged metal cations to hydrogen.[29,34−38] In this work, we extend the doped metals in COFs to three groups of alkali (Li, Na, and K), alkaline-earth (Be, Mg, and Ca), and transition (Sc and Ti) metals for enhancing $CO_2$ capture, in particular. To choose ideal metal modifiers for $CO_2$ capture in porous materials, we first compared the binding energies of a $CO_2$ molecule with the positively charged metal atoms, $M^+$ ($M$ = Li, Na, K, Be, Mg, Ca, Sc, and Ti), by using the first principles calculations, which were performed at the theoretical level of MP2/6-311G** with the BSSE correction. It is found from Table 1 that all the positively charged metal cations show very strong affinity to a $CO_2$ molecule. For the alkali metals, the calculated binding energies of a $CO_2$ molecule with $Li^+$, $Na^+$, and $K^+$ are −19.752, −12.315, and −8.773 kcal/mol, respectively. For the alkaline-earth metals of $Be^+$, $Mg^+$, and $Ca^+$, they are −34.383, −14.751, and −11.409 kcal/mol, respectively, higher than the values for the alkali metals in the same row of the periodic table of the elements (PTE). Unfortunately, the alkaline-earth metals display much stronger electronegativity than the alkali metals in the same row in PTE, and thus, it is more difficult for them to lose valence electrons. As to the transition metals, $Sc^+$ and $Ti^+$, their interactions with a $CO_2$ molecule are very strong and reach −34.405 and −66.764 kcal/mol, respectively. Generally, the order of magnitude of physisorption heat is defined as lower than about 5 kcal/mol (~20 kJ/mol), while that of chemisorption heat is defined as higher than about 12 kcal/mol (~50 kJ/mol). Apparently, most of the studied metal cations interact with a $CO_2$ molecule by chemisorption. The above analysis indicates that the key factor of enhancing $CO_2$ adsorption in porous materials is the cationization of the selected metals.

Subsequently, we further studied the doping of the selected metal atoms in COFs and compared their effect on $CO_2$ capture. As mentioned above, the DFT method like PW91 is much more efficient than the high-level MP2 method in solving large systems, while often provides comparable results to the MP2 level. Therefore, in our following work, the adsorption of $CO_2$ molecules and metal atoms in COFs was investigated by using the combined PW91/6-311g(d,p)//B3LYP/6-31 g(d) method, in which the latter was used for geometry optimizations and the former for the following potential energy calculations. To test the reliability of this combined method, we also calculated the binding energies between the metal cations and $CO_2$ by the combined method, and also listed in Table 1. Our results indicate that the PW91/6-311g(d,p)//B3LYP/6-31g(d) combined method gives comparable results to the high-level MP2 method, especially for the alkali metals. For alkaline-earth and transition metals, this method also provides reasonable tendency for the interactions between $CO_2$ and metal cations. Consequently, it is believed that the PW91/6-311g(d,p)//B3LYP/6-31g(d) combined method can be used to evaluate the adsorption of $CO_2$ and metal atoms in COFs.

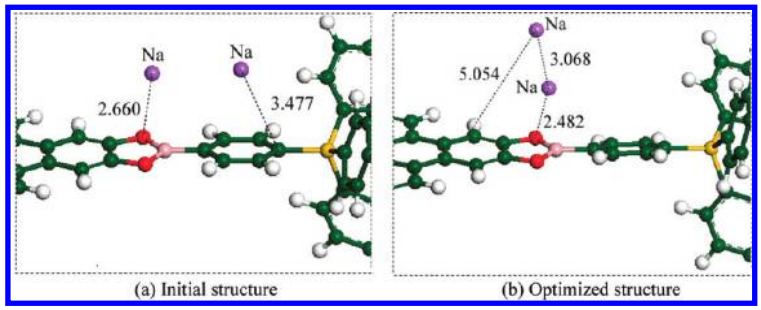


**Figure 5. The adsorption geometries of two Na atoms in COFs: (a) The initial structure, and (b) The optimized structure. The calculated binding energy of two Na atoms in COFs shown in (b) is −22.625 kcal/mol. The measured distances from the adsorbed Na atoms to the surface are presented in Å. C, O, B, H, Si, and Na atoms are shown as green, red, pink, white, yellow, and purple colors, respectively.**

***Comparison of Metals Doped in COFs.*** In our previous work,[29] adsorption of single and multiple Li atoms in COFs has been extensively studied. It is found that the top of the phenyl in COFs is the most favorable adsorption site for Li atoms. On the COFs surface, the doped Li atoms tend to be positively charged due to the charge transfer to the framework surfaces. However, excessive dop-

ing of Li atoms to COFs may also lead to the clustering effect and thus decreases the adsorption capacity of hydrogen.[29] Here, the adsorption of alkali metals, Na and K, the alkaline-earth metals, Be, Mg, and Ca, as well as the transition metals, Sc and Ti, in COFs was further studied for comparison.

As illustrated above, the COFs were synthesized by using three molecular building blocks: TBPS, TBPM, and HHTP (Figure 1). Among these crystalline frameworks, COF-105 possesses nearly all the representative adsorption positions. Therefore, a big fragment in COF-105 was adopted to represent the possible adsorption sites of metal atoms, and the broken bonds of the selected fragment were terminated by H atoms. Figure 3 shows the selected cluster model used in this work, from which we can see that there are mainly seven possible adsorption sites for metal atoms. Among the seven sites, sites α, δ, and β exist in all the four COF materials, while sites θ, γ, η, and μ only exist in COF-105 and COF-108. Here, θ is similar to the top site of the $B_3O_3$ rings in COF-102 and COF-103. In our first-principles calculations, the terminal atoms of the fragment were frozen to remain the constraints from the 3D crystal lattices. The geometry optimizations were performed with the hybridized B3LYP method and the 6-31G* basis set. The binding energies and the electrostatic potential fitting (ESP) charges were calculated by the high-quality PW91/6-311G** method. Note that the PW91 exchange-correction functional has been widely used in previous works due to its good performance in energy prediction.[39−41] The binding energy, B.E., between the doped metal atoms and the COFs is defined as

$$\text{B.E.} = E(\text{nM/host}) - E(\text{host}) - nE(\text{M}) \qquad (1)$$

where $n$ denotes the number of the coadsorbed metal atoms, while $E$(nM/host), $E$(host), and $E$(M) denote the energies of the adsorption complexes, the host material, and the metal atom, respectively.

In the geometry optimizations, each site labeled in Figure 3 is considered as possible occupancy of the metal atoms. It is found from our calculations that θ and μ are the most unfavorable adsorption positions for all the alkali, alkaline-earth, and transition metals studied here. Our first-principles calculations indicate that a single metal atom placed at θ (the top of $C_2O_2B$ or $B_3O_3$ ring) will migrate to the neighboring β after optimization. In addition, all the metal atoms studied in this work can not be stably located at site μ on the HHTP building block and will move to η or γ after optimization, because all the carbon atoms of the center hydrocarbon ring in the HHTP building block are charged with a small amount of positive charges; thus, the interactions between the π electrons of the center hydrocarbon ring and the located metal atoms are weaker than those for the surrounding hydrocarbon rings.

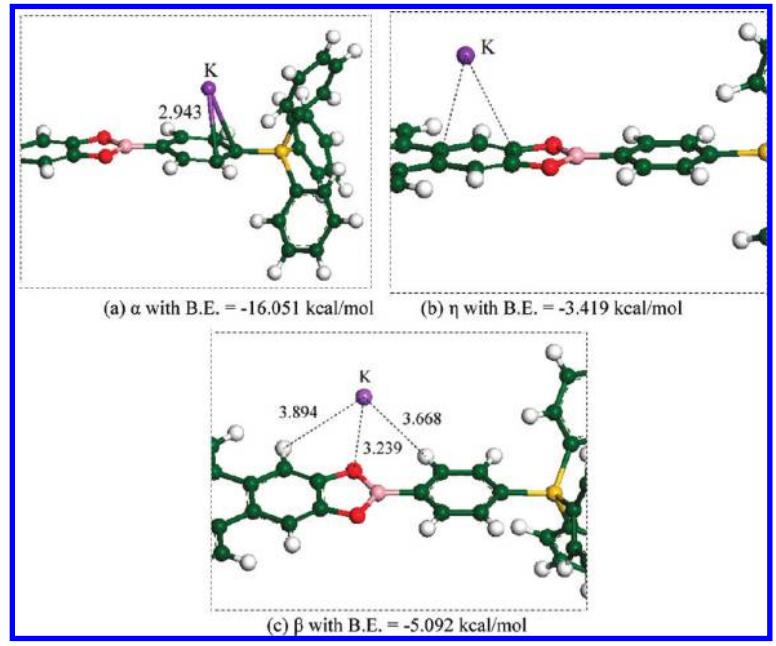


**Figure 6. Optimized adsorption sites and binding energies of K in 3D COFs: (α) α, (b) η, and (c) β. The structure deformation is seen in (a) from the slight bending of the framework. The measured distances from the adsorbed K atom to the surface are presented in Å. C, O, B, H, Si, and K atoms are shown as green, red, pink, white, yellow, and purple, respectively.**

***Adsorption of Alkali Metals in COFs.*** As mentioned above, there are a series of possible adsorption sites in COFs for metal atoms. Because the configuration of Li adsorption in COFs has been studied extensively,[29] we just discuss the possible adsorption sites and the corresponding binding energies of the other two alkali metals, Na and K, in this section.

Figure 4 gives all the optimized adsorption geometries of Na in COFs derived from our first principles calculations. Our results show that there are mainly three adsorption positions for a single Na atom, that is, α on

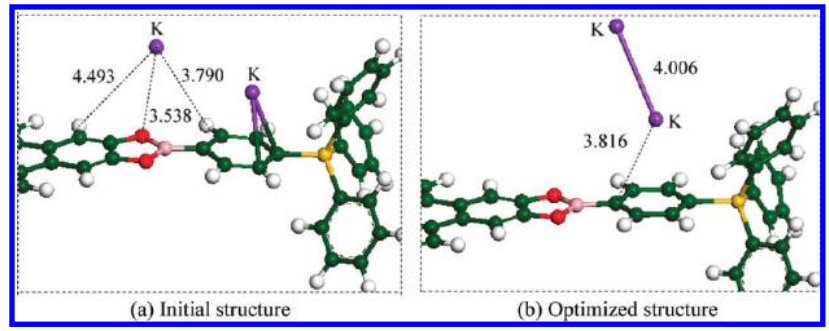


**Figure 7. Adsorption geometries of two K atoms in COFs: (a) initial structure and (b) optimized structure. The binding energy of two K atoms in COFs is −18.414 kcal/mol. The measured distances from the adsorbed K atoms to the surface are presented in Å. C, O, B, H, Si, and K atoms are shown as green, red, pink, white, yellow, and purple colors, respectively.**

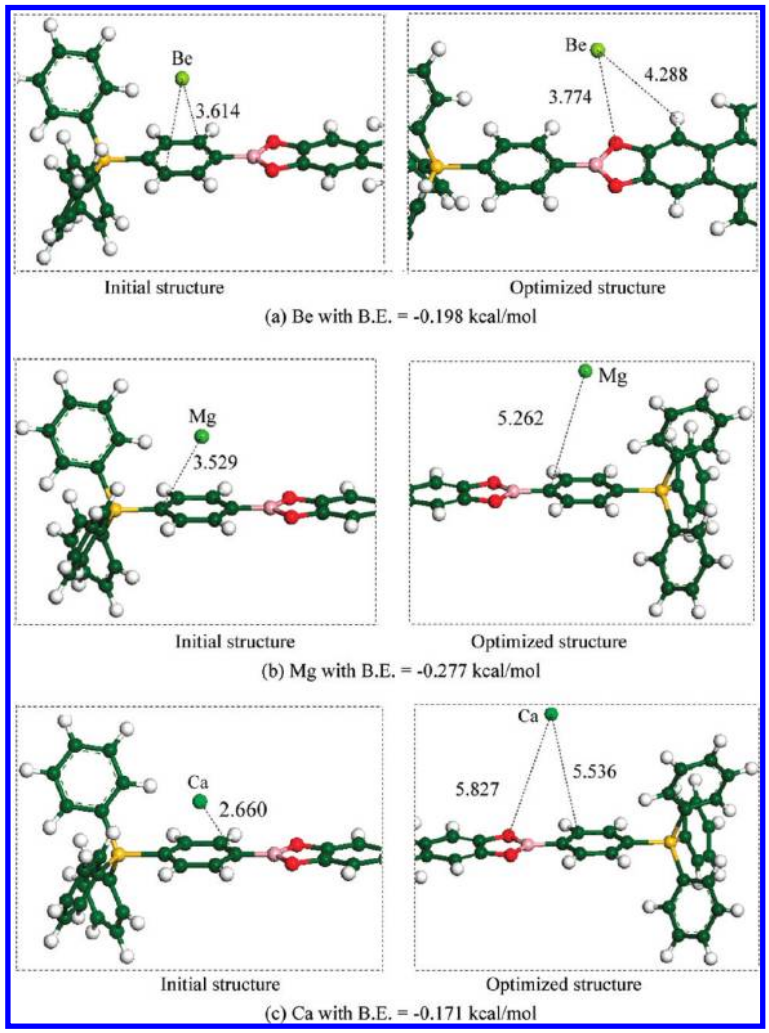


**Figure 8. Optimized adsorption sites and binding energies of alkaline-earth metals in COFs: (a) Be, (b) Mg, (c) Ca. The measured distances from the adsorbed Be, Mg, and Ca atoms to the surface are presented in Å. C, O, B, H, and Si atoms are shown as green, red, pink, white, and yellow colors, respectively.**

the TBPS/TBPM building block, η on the HHTP building block, and β near the oxygen atom of the $B_3O_3$ or $C_2O_2B_2$ ring. At these sites, the calculated binding energies are −6.882, −2.064, and −2.371 kcal/mol, respectively, suggesting that a single Na atom prefers first to locate at the top of a single phenyl ring on the COF surface. The calculated ESP charge loaded by a Na atom at α is +0.435|*e*|, while those for Na atom at η and β are nearly zero.

An interesting observation is that, if two Na atoms are separately placed at the neighboring α and β sites, the Na atom at α site would translate to β and clusters together with that at β after geometry optimization (Figure 5). The calculated binding energy of two Na atoms with COFs reaches −22.625 kcal/mol, indicating that the dispersed neutral Na atoms prefer to form a cluster in COFs.

Figure 6 gives the calculated possible adsorption sites for a single K atom in COFs. It is found that a single K atom also prefers to locate at α, η, and β like Na. At those sites, the calculated binding energies are −16.051, −3.419, and −5.092 kcal/mol, respectively. Clearly, α is more favorable than other two sites for a K atom. The calculated ESP charge loaded by a K atom at α site is 0.638|*e*|, while those for the atoms at η and β are nearly zero. It is noticeable that adsorption of K exerts obviously stronger stress to the framework than that of Li and Na, which can be observed from the slight bending deformation of the framework shown in Figure 6a.

Figure 7 shows the initial and optimized coadsorption modes of two K atoms in COFs. As shown in Figure 7a, two K atoms in the initial structure were placed at α and β, respectively. After geometry optimization, the dispersed K atoms form a cluster with a binding energy of −18.414 kcal/mol. Consequently, K is not suitable for modification of COFs in $CO_2$ capture either.

***Doping of Alkaline-Earth Metals in COFs.*** Our first principle calculations indicate that Be, Mg, and Ca atoms can not be stably adsorbed at the COFs surface. When a Be atom is placed at the α site in the initial structure, it translates to the adjacent β with the binding energy of just −0.198 kcal/mol (Figure 8a,b). In addition, Mg and Ca atoms also weakly interact with COFs. As a result, all the calculated binding energies of Be, Mg, and Ca with COFs are lower than −0.3 kcal/mol, which is too weak for them to be stably adsorbed.

***Doping of Transition Metals in COFs.*** It is reported that the transition metals, such as Sc and Ti, are possible modifiers for porous materials in hydrogen storage.[42−45] Accordingly, we further studied the doping of transition metals, Sc and Ti, in COFs in this work.

Figure 9 shows the calculated possible adsorption sites of Sc in COFs, where the binding energies are also presented. As shown in Figure 9a, a single Sc atom prefers to be adsorbed at α on the TBPS or TBPM building block with a large binding energy of −51.188 kcal/mol. When adsorbed at η on the HHTP building block (Figure 9b), the obtained binding energy of Sc with COFs is −46.747 kcal/mol. In contrast, when the Sc atom is adsorbed at β, the calculated binding energy is just −5.612 kcal/mol, suggesting that the probability of Sc atoms existing at β is far lower than these at α and η (Figure 9c). Sc, the first transition element, has the valence electron configuration of $3d^1s^2$, suggesting that its valence electrons can be easily lost or redistributed during hybridization. Hence, the Sc atoms adsorbed at α and η are positively charged with the ESP charges of 0.867|*e*| and 0.639|*e*|, respectively, while it is negatively charged at β with −0.148|*e*|.

Figure 10 shows the calculated possible adsorption sites of Ti in COFs and the corresponding binding ener-

gies. Compared to the metals studied previously, the Ti atom shows the strongest interaction with COFs. For Ti atoms, site α on the TBPS or TBPM building block is the most favorable adsorption position with a binding energy of −105.727 kcal/mol (Figure 10a). At η on the HHTP building block, the calculated binding energy of Ti with COFs reaches −81.388 kcal/mol, while that at β is only −10.785 kcal/mol. Clearly, a Ti atom can bind with the framework of COFs strongly. As shown in Figure 10d, a Ti atom can even bind with two neighboring carbon atoms in the phenyl with a binding energy of −56.359 kcal/mol. The valence electron configuration of Ti is $3d^2s^2$, which makes the Ti atom very active in chemical reactions. The calculated ESP charges of Ti atoms adsorbed at α and η are 0.872|*e*| and 0.296|*e*|, respectively, while it is nearly neutral at β. If a Ti atom is bound to two neighboring carbon atoms of the phenyl (Figure 10d), it will also be positively charged with a quantity of 0.194|*e*|.

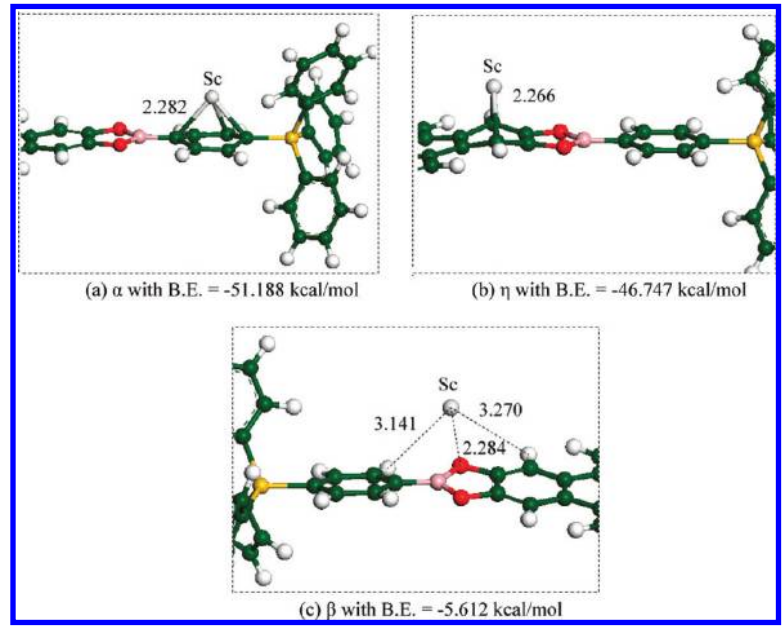


**Figure 9. Optimized adsorption sites and binding energies of Sc in COFs: (a) α, (b) η, and (c) β. Partial structure deformations are seen in (a) and (b). The measured distances from the adsorbed Sc atoms to the surface are presented in Å. C, O, B, H, Si, and Sc atoms are shown as green, red, pink, white, yellow, and silver colors, respectively.**

***Brief Summary on Doping of Metals in COFs.*** As mentioned above, the doping of several alkali, alkaline-earth, and transition metals, including Li, Na, K, Be, Mg, Ca, Sc, and Ti, was systemically studied by using the first principles calculations. Our results indicate that the phenyl of the TBPS and TBPM building blocks in COFs offers the most favorable adsorption site (i.e., site α) for all metals studied here.

For the alkali metals, Li, Na, and K, the Li atom can be adsorbed at the most adsorption sites in COFs and can stably bind with COFs in energy, while adsorption of Na and K is relatively unstable due to their low binding energies with the host material. As listed in Table 2, the binding energies of Li, Na, and K atoms doped at the α site in COFs are −23.70, −6.88, and −16.05, respectively. In addition, the doped Na and K atoms are more likely to form a cluster in COFs. For the alkaline-earth metals, Be, Mg, and Ca, they interact with COFs weakly and thus their binding with COFs is unstable. In contrast, the calculated binding energies of the transition metals, Sc and Ti, are significantly higher than those for the alkali and alkaline metals. Consequently, the strong interaction would lead to some structure deformation of the host materials

**Impact of Metal-Doping on $CO_2$ Capture.** ***Adsorption of $CO_2$ in Li-Doped COFs.*** Because Li, Sc, and Ti can be stably attached to the frameworks of COFs, we further focus on the effect of their doping on $CO_2$ capture. Figure 11 displays the optimized adsorption geometries of single and three $CO_2$ molecules in the Li-doped COFs, respectively. As shown in Figure 11a, when a Li atom, doped at the top of the phenyls in the TBPS or TBPM building block, is positively charged, it can adsorb one $CO_2$ molecule with the calculated binding energy of −10.074 kcal/mol, where $CO_2$ nearly lies on the surface with the O−Li distance of 1.976 Å. Obviously, the modification of COFs with Li cations enhances the affinity of the host material to $CO_2$ significantly, compared to the nondoped ones, in which the absolute values of the $CO_2$−COFs interaction are in the range of approximately 0−4 kcal/mol. It is noticed that the binding en-

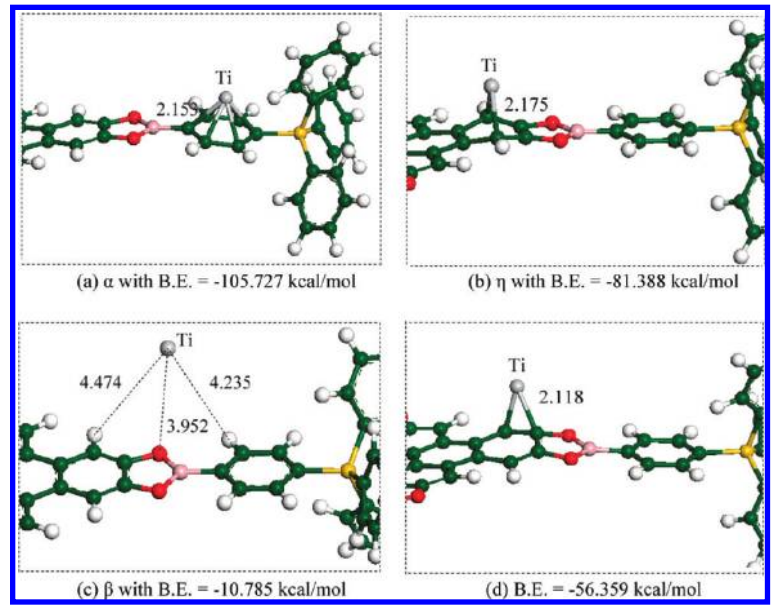


**Figure 10. Optimized adsorption sites and binding energies of Ti in COFs: (a) α, (b) η, and (c) β. Partial structure deformations are seen in (a), (b), and (d). The measured distances from the adsorbed Ti atoms to the surface are presented in Å. C, O, B, H, Si, and Ti atoms are shown as green, red, pink, white, yellow, and silver colors, respectively.**

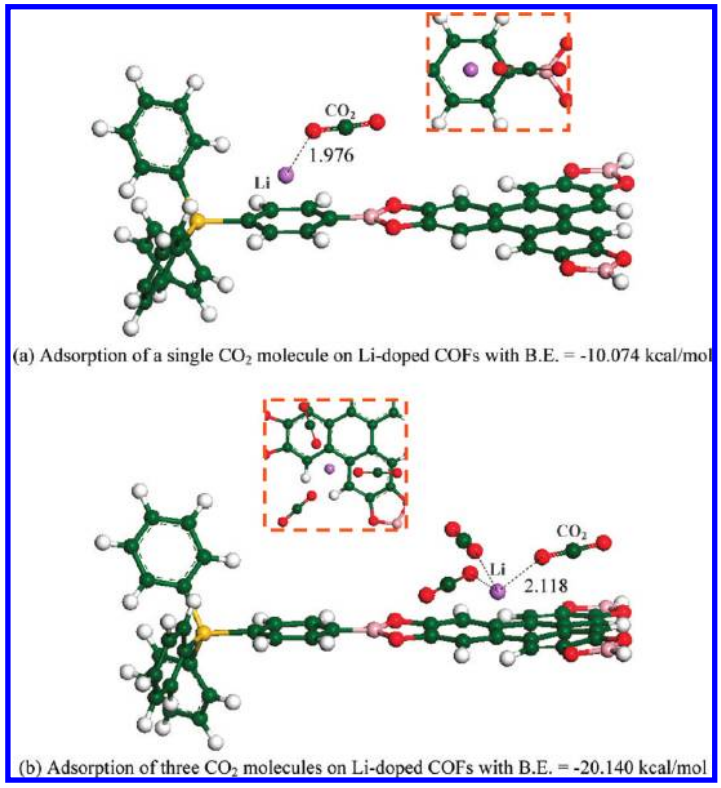


**Figure 11. Optimized adsorption geometries of (a) single and (b) three $CO_2$ molecules in the Li-doped 3D COFs. The top views of the optimized geometries are shown in the insets. The calculated binding energies are also presented. The measured distances from the adsorbed $CO_2$ molecules to the Li atom are shown in Å. C, O, B, H, Si, and Li atoms are shown as green, red, pink, white, yellow, and purple colors, respectively.**

ergy of $CO_2$ with the Li-doped COFs exceeds the upper limit of physisorption (~5 kcal/mol or 20 kJ/mol), while it is still below the lower limit of chemisorption (~12 kcal/mol or 50 kJ/mol).

To explore the interaction mechanism between $CO_2$ and a Li cation, we further studied the highest occupied molecular orbital (HOMO) of the adsorption complex, $CO_2$/Li/COF-105, where the Li cation is doped on the top of the phenyl in the TBPS building block (Figure 12). For comparison, the HOMO of the $CO_2/Li^+$ interaction system is also presented. As shown in Figure 12a, the hybridization between $CO_2$ and the doped Li cation is very weak, which indicates that their strong binding energy mainly originates from the nonbonded electrostatic ion···quadrupole of $CO_2$ interaction. Actually, the $CO_2$ molecule is slightly polarized when it is adsorbed around the Li cation after optimization. The nonbonded interaction between the electrostatic cation and the quadrupole of $CO_2$ also dominates the interaction between a $CO_2$ molecule and a naked $Li^+$ (Figure 12b).

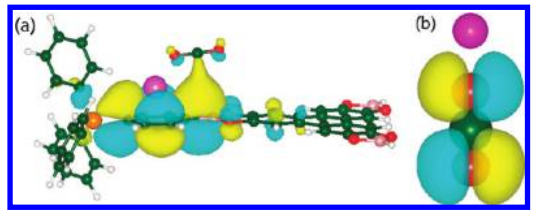


**Figure 12. Highest occupied molecular orbital (HOMO) for the interaction of a $CO_2$ molecule with (a) the Li-doped COFs and (b) a naked $Li^+$ cation. C, O, B, H, Si, and Li atoms are shown as green, red, pink, white, yellow, and purple colors, respectively.**

Additionally, we studied the adsorption geometries of three $CO_2$ molecules around one Li cation in COFs. If a Li atom is loaded at site γ on the HHTP building block, it will also be positively charged as is proved in our previous work due to the charge transfer to the surface.[29] Figure 11b displays the optimized structure, from which it is found that the adsorbed three $CO_2$ molecules lie simultaneously on the surface with one end toward the Li cation. The distances of the Li cation to the nearest O in $CO_2$ are 2.118, 2.114, and 2.130 Å, respectively. The calculated total binding energy reaches −20.140 kcal/mol, which indicates that the Li atom doped on the HHTP building block can stably adsorb at least three $CO_2$ molecules.

***Adsorption of $CO_2$ in Sc- and Ti-Doped COFs.*** In this section, we discuss the interaction between $CO_2$ molecules and a Sc atom loaded in COFs. Figure 13a presents the optimized adsorption geometries of a $CO_2$ molecule on the Sc-doped COFs. As mentioned above, a single Sc atom adsorbed on the top of phenyls in the TBPS or TBPM building block can easily lose its valence elections. Our results show that the binding energy between a $CO_2$ molecule and a Sc cation dispersed in COFs is −14.042 kcal/mol (nearly −58.406 kJ/mol), stronger than the lower limit of chemisorption (~12 kcal/mol or 50 kJ/mol). In addition, the distance between the Sc cation and the nearest O atom in $CO_2$ is 2.350 Å. Figure 13b displays the optimized adsorption geometries of a $CO_2$ molecule around a doped Ti cation in COFs. The calculated binding energy of $CO_2$ with the Ti-doped COFs is −15.410 kcal/mol, and the distance between the Ti cation and the nearest O atom in $CO_2$ is 2.229 Å. That is to say, both the doped Sc and Ti cations interact with $CO_2$ by chemisorption and, thus, would suffer from the difficulty of desorption.

***Brief Summary on $CO_2$ Adsorption in Metal-Doped COFs.*** In summary, among the alkali, alkaline-earth, and transition metals studied, Li, Sc, and Ti can promote the adsorption capacity of $CO_2$ in COFs significantly. However, the binding energies of a $CO_2$ molecule with the transition metal cations, Sc and Ti, exceed the lower limit of chemisorption, and would suffer from the difficulty of

**TABLE 2. Binding Energies between a Metal Atom and COFs from the First-Principles Calculations**

| site | Li | Na | K | Sc | Ti |
|---|---|---|---|---|---|
| α | −23.70 | −6.88 | −16.05 | −51.188 | −105.727 |
| β | −8.87 | −2.37 | −3.40 | −5.612 | −10.785 |
| η | −14.47 | −2.06 | −5.09 | −46.747 | −81.388 |
| γ | −14.71 | | | | |
| δ | −16.16 | | | | |
| θ | | | | | |
| μ | | | | | |

desorption. In contrast, the interaction of $CO_2$ with Li cations is in the range between physisorption and chemisorption, and thus, the adsorption and desorption are reversible at room temperature. In conclusion, the Li atom is the best modifier of COFs among all the metals studied here for capturing $CO_2$ effectively.

***Adsorption of $CO_2$ in Li-Doped COFs at $T = 298$ K.*** On the basis of the above work, we further predicted adsorption of $CO_2$ in the Li-doped COFs at room temperature. The doping scheme of Li in COFs can be referred to our previous work,[29] in which all the Li atoms are positively charged. In our distribution scheme, eight Li atoms are placed at site α and δ on the TBPM or TBPS building block, respectively, as is shown in Figure 14, while just one Li atom is placed at site γ on the HHTP building block.

***Interaction between $CO_2$ and Li Cations.*** To obtain the interaction energies between $CO_2$ and the doped Li cation in COFs, a series of single point energy was calculated by high-quality PW91/6-311G** including the BSSE correction. By fitting the discrete potential energies to the mixed potential function in eq 2, the force field parameters for the interaction between $CO_2$ and the Li cation were thus derived (see Supporting Information). The comparison of the $CO_2$−Li cation interaction energies, derived from the first-principles and our fitted force field parameters, are presented in Supporting Information (see Figure S1), from which the good agreement can be observed.

***Adsorption of $CO_2$ in Li-Doped COFs.*** The adsorption isotherms of $CO_2$ in the Li-doped COFs at $T = 298$ K were evaluated by using GCMC simulation. In our simulation, the atomic charges of the frameworks were also taken into consideration. According to our previous first principles calculations,[29] the ESP atomic charges of the doped Li atoms in our distribution scheme are positively charged in the range from 0.30|*e*| to 0.45|*e*|. Therefore, by fixing the ESP charges of the doped Li atoms, those of the other atoms in the unit cells of the Li-doped COFs were then determined by using the QEq method.

Figure 15 presents the simulated excess gravimetric and volumetric uptakes of $CO_2$ in the Li-doped COFs at $T = 298$ K. By modifying COFs with Li, the performances of COFs for $CO_2$ capture are significantly improved compared to the nondoped counterparts, especially at the low pressures (see the inset in Figure 15a). The simulated gravimetric $CO_2$ uptakes for nondoped and Li-doped COFs at representative pressures are summarized in Table 3, and these data for several MOFs of high $CO_2$ uptakes are also presented for comparison. As listed in Table 3, the gravimetric uptakes of $CO_2$ in the Li-doped COF-102 and COF-105 reach 409 and 344 mg/g at $T = 298$ K and $p = 1$ bar, which are about eight and four times those for the nondoped counterparts (52 mg/g for COF-102; 93 mg/g for COF-105), respectively. Compared to the MOFs, which are among the highest scores of $CO_2$ capture at present, the $CO_2$ adsorption capacities of the Li-doped COFs are even superior (Table 3). As the pressure increases to 5 bar, the gravimetric $CO_2$ uptakes of the Li-doped COF-102 and COF-105 are 841 and 703 mg/g, respectively, still significantly higher than the nondoped materials. Note that the gravimetric $CO_2$ uptakes of the Li-doped COF-105 is far from saturation at low and moderate pressures due to its exceptional large free volume (88.42%)[29] and low density (0.18 g/cm$^3$). In particular, at $p = 40$ bar, the excess gravimetric uptake of $CO_2$ in Li-doped COF-105 reaches 2266 mg/g, while it is 1773 mg/g for the nondoped COF-105. Consequently, the modification of COFs by Li-doping enhances pronouncedly their $CO_2$ uptakes at very low pressures. The excess volumetric uptakes of $CO_2$ in Li-doped COFs are also presented in Figure 15b, from which we can see that the Li-doped COF-102 shows greatly higher $CO_2$ volumetric uptakes than the Li-doped COF-105 due to the relative small pore size of COF-102. At 20 bar, the volumetric uptake of $CO_2$ in Li-doped COF-102 reaches 313 V(STP)/V, while it is only 139 V(STP)/V for Li-doped COF-105. Obviously, the Li-doping modification greatly enhances the $CO_2$ capacity of COFs. In one word, the Li-doped COFs are the most promising candidates for $CO_2$ capture at present.

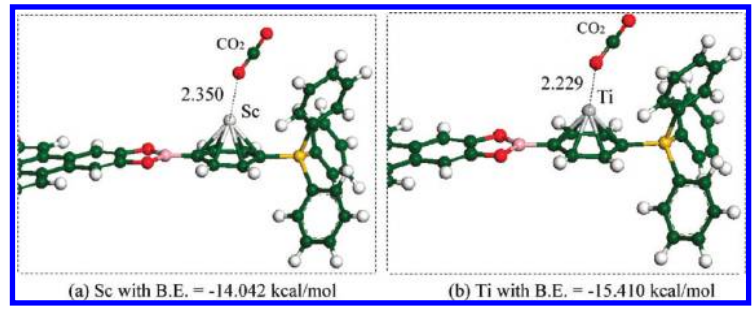


**Figure 13. Optimized adsorption sites and binding energies of $CO_2$ in (a) Sc- and (b) Ti-doped 3D COFs. The measured distance from the adsorbed $CO_2$ molecule to the Sc or Ti atom is presented in Å. C, O, B, H, and Si atoms are shown as green, red, pink, white, and yellow colors, respectively.**

## CONCLUSIONS

In this work, we have used the multiscale simulation approach, which combines the first-principles calculations and molecular simulation, to comprehensively study the doping of a series of alkali (Li, Na, and K), alkaline-earth (Be, Mg, and Ca), and transition (Sc and Ti) metals in COFs, and the effects of the doped metals on $CO_2$ capture. Our results indicate that the phenyl of the TBPM and TBPS building blocks in COFs provides the most favorable adsorption locations for all the metals studied. For the alkali metals, Li, Na, and K, the Li atom can be doped in the most adsorption sites in COFs and can stably bind with COFs, while the adsorption of Na and K is relatively unstable due to the low binding energies. Moreover, the doped Na and K atoms prefer

to form clusters in COFs. For the alkaline-earth metals, Be, Mg, and Ca, the interaction energies with COFs are weak, and thus, their binding with COFs is unstable. In contrast, the binding energies of the transition metals, Sc and Ti, are much higher than the alkali and alkaline-earth metals and would, on the other hand, lead to the structure deformation of the host materials.

By further exploring the effects of the doping of the metals mentioned above on $CO_2$ adsorption, it is found that, among all the metals studied, Li, Sc, and Ti can significantly improve the adsorption capacity of $CO_2$ in COFs. However, the binding energy of a $CO_2$ molecule with the transition metals, Sc and Ti, exceeds the lower limit of chemisorptions and, thus, suffers from the difficulty of desorption. In contrast, the interaction of $CO_2$ with Li cations is within the range between physisorption and chemisorption, and thus, the adsorption and desorption are reversible at room temperature. By the comparative studies above, it is concluded that Li is the best surface modifier of COFs for $CO_2$ capture among all the metals studied, because Li can be stably bound to the framework surface. Furthermore, Li has a light weight, easily loses its valence electrons, and therefore, improves the affinity of host materials toward $CO_2$. For example, the binding energy between a $CO_2$ molecule and the COFs is about −4.00 kcal/mol at most, while that between a $CO_2$ molecule and the Li-doped COFs is −10.074 kcal/mol, which is greatly enhanced due to the electrostatic interaction between a $CO_2$ molecule and the Li cation.

Accordingly, we further investigate the uptakes of $CO_2$ in the Li-doped COFs. Our GCMC simulation results show that doping of Li in COFs can significantly improve the $CO_2$ uptakes at 298 K due to the strong binding energy between $CO_2$ and Li cations, especially at low pressures. It is found that at 298 K and 1 bar, the excess $CO_2$ gravimetric uptakes of the Li-doped COF-102 and COF-105 reach 409 and 344 mg/g, respectively, which are about eight and four times those in the non-doped frameworks (52 mg/g for COF-102; 93 mg/g for COF-105), respectively. Impressively, the Li-doped COF-105 presents the $CO_2$ gravimetric uptake up to 2266 mg/g at 40 bar, which is the highest score reported so far.

In short, doping of metals in high performance covalent organic frameworks provides an efficient approach for enhancing $CO_2$ capture. The mechanisms of doping have been explored through extensive first-principles calculations and molecular simulations in this work. It is expected that the results would help the preparation and development of new materials for adsorptive capture of $CO_2$ in the future.

## MODELING AND COMPUTATIONAL DETAILS

Before the doping of metals, the 3D structures of COFs were first constructed according to the reported structural information.[1] To predict $CO_2$ adsorption in COFs, a multiscale simulation method, which combines the first-principles calculation and GCMC simulation, was used in this work. The multiscale method consists of the following procedures: (a) to calculate the interaction between $CO_2$ and the host materials; (b) to parametrize the calculated interaction energies by force field fitting; and (c) to predict the adsorption capacities of $CO_2$ in the host materials with the force field parameters obtained here.

As is well-known, the unit cells of the 3D COFs are very large (see Figure 1), which make it unrealistic to investigate COFs with the first principles calculations. Therefore, the commonly used cluster model method was adopted here to represent the real structure of COFs for reducing computational cost. Four cluster models were used to represent the atom types in COFs (Figure 1). $C_6H_6$ and $B_3O_3H_3$ were mainly used to represent the $sp^2$ hybridized C and B as well as the O atoms in COFs, while $C_9H_{12}$ and $Si_3C_6H_{12}$ were used to represent the $sp^3$ hybridized C and Si atoms, respectively. The nonbond interaction energies between $CO_2$ and the cluster models were calculated by the high-quality MP2/cc-PVTZ method,[46−49] including the basis set superposition error (BSSE) correction. All the first-principles calculations were performed with the Gaussian 03 software.[50] Using the calculated interaction energies, the force field parameters for the nonbond interaction between $CO_2$ and COFs can thus be fitted.

For adsorption of alkali, alkaline-earth, and transition metals in COFs, the geometry optimization was performed with the hybrid density functional B3LYP[51,52] and the 6-31G (d) basis set. As is well-known, the B3LYP hybrid functional is the most widely used functional in geometry optimizations, especially for the sys-

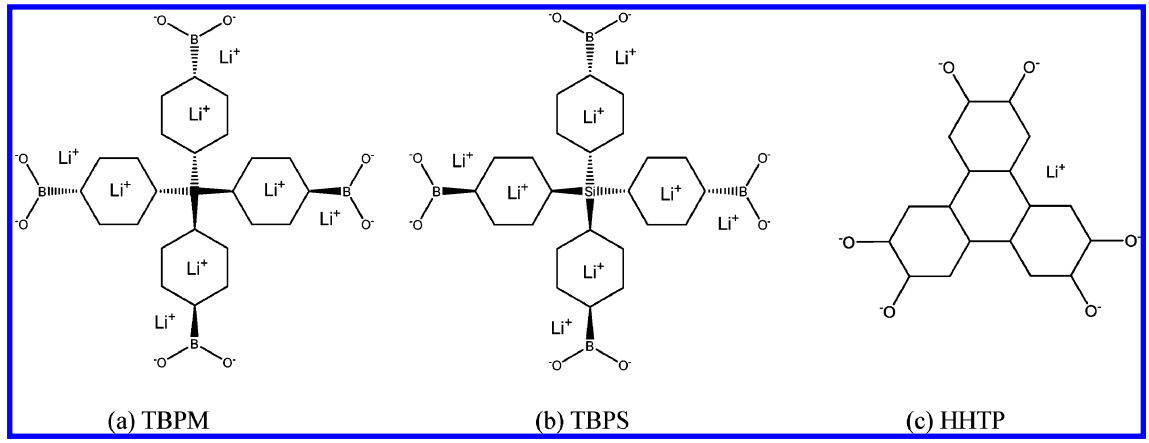


**Figure 14. Distribution scheme of Li atoms on the building blocks of 3D COFs, in which H atoms bonded to O are neglected for clarity: (a) TBPM, (b) TBPS, and (c) HHTP.**

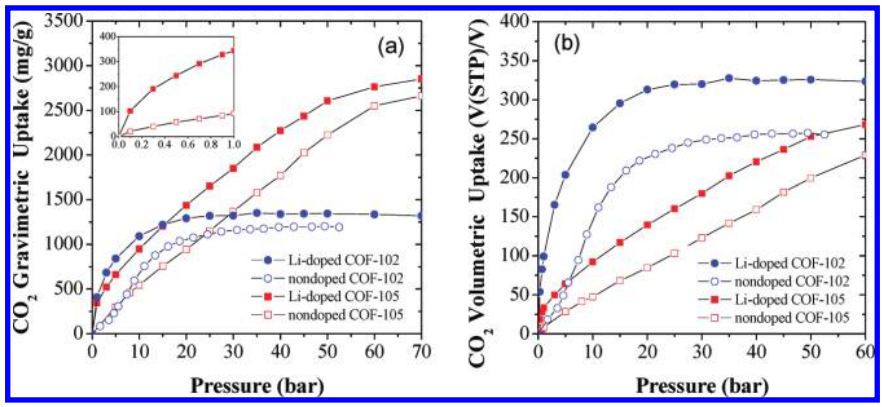


**Figure 15. Simulated excess in (a) gravimetric and (b) volumetric isotherms of $CO_2$ in the Li-doped COFs at $T = 298$ K. For comparison, the data for the nondoped COFs are also presented. In addition, the inset in (a) shows the simulated excess $CO_2$ uptakes in the nondoped and Li-doped COF-105 in the pressure range of 0−1 bar at 298 K.**

tems containing metal atoms.[53] The binding energies and the electrostatic potential fitting (ESP) charges were calculated by the pure PW91 functional, as reported previously.[29] It is worth mentioning that, to date, many works have shown that pure DFT functionals, such as PW91 and PBE, can often give good qualitative results in evaluating noncovalent interactions such as van der Waals (vdW) interactions in molecular complexes and in the solid state.[25,54−59] For example, Wesolowski *et al.* studied the binding energies and geometries of benzene with $O_2$, $N_2$, and CO and found that PW91 can give results comparable in accuracy to the high-level MP2/6-31G** method.[43] In addition, the ESP charges were obtained by using the Merz−Kollman scheme (MK).[60,61] In applying the MK scheme, the minimum exclusion radii of K, Ca, Sc, and Ti were set to 1.5 times of their atomic vdW radii in this work.

A three-site rigid molecular model is used to represent $CO_2$, and its quadrupole moment is described by a partial-charge model. In the $CO_2$ molecular model (Figure 1), the C−O bond is 1.18 Å in length and the bond angle is 180°. The partial charges loaded by C and O are $q_C = +0.70e$ and $q_O = -0.35e$, where $e = 1.602 \times 10^{-19}$ C. For $CO_2$−$CO_2$ and $CO_2$−COFs interactions, the nonbond potential energy $U_{ij}$ is represented by the combination of the Lennard-Jones (LJ) potential and the Coulombic potential given by

$$U_{ij}(r_{ij}) = 4\varepsilon\left[\left(\frac{\sigma}{r_{ij}}\right)^{12} - \left(\frac{\sigma}{r_{ij}}\right)^{6}\right] + \frac{q_i q_j}{r_{ij}} \qquad (2)$$

where $r_{ij}$ is the distance between atoms $i$ and $j$. The parameters $\varepsilon$ and $\sigma$ are the energy well depth and vdW radius, respectively, derived from the Lorentz−Berthelot mixing rules $\varepsilon = \sqrt{\varepsilon_i \times \varepsilon_j}$ and $\sigma = (\sigma_i + \sigma_j)/2$. The pairwise electrostatic interaction was calculated by using the atomic charges, $q_i$ and $q_j$. For the complexity of charge distribution, both the atomic charges in the four cluster models and COFs were calculated by using the charge equilibration (QEq) method for consistency.[62] In the metal-doped COF compounds, the charges of the doped metal atoms were calculated by the first-principles calculations, and then those of the other atoms in the frameworks were approximately determined by the QEq method.

When the fitted force field parameters are used as input, the GCMC simulations were then performed to evaluate the adsorption isotherms by specifying temperature, volume, and chemical potential first. The Widom's test particle insertion method in a NVT ensemble was used to describe the relationship between chemical potential and pressure, as was used previously.[28−30] To eliminate the boundary effect, the periodic boundary conditions were applied in all three dimensions. During the GCMC simulations, one unit cell of the studied COFs was adopted in the simulation box. The LJ interaction beyond half of the simulation box was neglected during our GCMC simulations. For the Columbic interactions, the Ewald sum was used with the real-space partition parameter of 0.2 $Å^{-1}$ to ensure the convergence. For each state point, the GCMC simulation consisted of $1 \times 10^7$ steps to guarantee equilibration, and the following $1 \times 10^7$ steps were used to sample the desired quantities. The total amount of $CO_2$ molecules adsorbed per unit cell $N_{tot}$ was converted to the excess adsorption amount by the following equation

$$N_{exc} = N_{tot} - \rho(T,P)V_{free} \qquad (3)$$

where $\rho(T,P)$ represents the density at the given temperature and pressure and $V_{free}$ is the free volume for adsorption. Here, $V_{free}$ was calculated as the volume within one unit cell, where the potential energy of interaction of a hydrogen molecule with the solid framework is less than $10^4$ K. The calculated free volumes for the adsorbents studied here were reported in our previous works.[29]

*Acknowledgment.* This work is supported by National Scientific Research Funding (ZD0901), Huo Yingdong Fundamental Research Foundation (121070), National Basic Research Program of China (2007CB209706), NSF of China (20736002), and Chemical Grid Program and Outstanding Talent Funding from BUCT.

**TABLE 3. Comparison of $CO_2$ Uptakes in Porous Materials**

| | $T = 298$ K | | | |
|---|---|---|---|---|
| materials | $p = 1$ bar | $p = 10$ bar | $p = 40$ bar | source |
| nondoped COF-102 | 52 | 685 | 1197 | this work |
| Li-doped COF-102 | 409 | 1092 | 1349 | this work |
| nondoped COF-105 | 93 | 554 | 1773 | this work |
| Li-doped COF-105 | 344 | 948 | 2266 | this work |
| MOF-5 | 44 | 479 | 970 | Millward and Yaghi[3] |
| MOF-177 | 35 | 497 | 1490 | Millward and Yaghi[3] |
| IRMOF-6 | 41 | 487 | 870 | Millward and Yaghi[3] |
| MIL-101(Cr) | 190 | 630 | 1760 (303 K, 50 bar) | Llewellyn *et al.*[16] |

*Supporting Information Available:* The fitted force field parameters and potential energy as well as the potential energy obtained from the first-principles calculations. This material is available free of charge *via* the Internet at http://pubs.acs.org.

## REFERENCES AND NOTES


1. El-Kaderi, H. M.; Hunt, J. R.; Mendoza-Cortes, J. L.; Cote, A. P.; Taylor, R. E.; O'Keeffe, M.; Yaghi, O. M. Designed Synthesis of 3D Covalent Organic Frameworks. *Science* **2007**, *316*, 268–272.
2. Furukawa, H.; Yaghi, O. M. Storage of Hydrogen, Methane, and Carbon Dioxide in Highly Porous Covalent Organic Frameworks for Clean Energy Applications. *J. Am. Chem. Soc.* **2009**, *131*, 8875–8883.
3. Millward, A. R.; Yaghi, O. M. Metal-Organic Frameworks with Exceptionally High Capacity for Storage of Carbon Dioxide at Room Temperature. *J. Am. Chem. Soc.* **2005**, *127*, 17998–17999.
4. Keskin, S.; Sholl, D. S. Screening Metal-Organic Framework Materials for Membrane-Based Methane/Carbon Dioxide Separations. *J. Phys. Chem. C* **2007**, *111*, 14055–14059.
5. Barcia, P. S.; Bastin, L.; Hurtado, E. J.; Silva, J. A. C.; Rodrigues, A. E.; Chen, B. L. Single and Multicomponent Sorption of $CO_2$, $CH_4$, and $N_2$ in a Microporous Metal-Organic Framework. *Sep. Sci. Technol.* **2008**, *43*, 3494–3521.
6. Bae, Y. S.; Mulfort, K. L.; Frost, H.; Ryan, P.; Punnathanam, S.; Broadbelt, L. J.; Hupp, J. T.; Snurr, R. Q. Separation of $CO_2$ from $CH_4$ Using Mixed-Ligand Metal-Organic Frameworks. *Langmuir* **2008**, *24*, 8592–8598.
7. Bastin, L.; Barcia, P. S.; Hurtado, E. J.; Silva, J. A. C.; Rodrigues, A. E.; Chen, B. A Microporous Metal-Organic Framework for Separation of $CO_2/N_2$ and $CO_2/CH_4$ by Fixed-Bed Adsorption. *J. Phys. Chem. C* **2008**, *112*, 1575–1581.
8. Thallapally, P. K.; Tian, J.; Kishan, M. R.; Fernandez, C. A.; Dalgarno, S. J.; McGrail, P. B.; Warren, J. E.; Atwood, J. L. Flexible (Breathing) Interpenetrated Metal-Organic Frameworks for $CO_2$ Separation Applications. *J. Am. Chem. Soc.* **2008**, *130*, 16842–16843.
9. Yazaydin, A. O.; Benin, A. I.; Faheem, S. A.; Jakubczak, P.; Low, J. J.; Willis, R. R.; Snurr, R. Q. Enhanced $CO_2$ Adsorption in Metal-Organic Frameworks *via* Occupation of Open-Metal Sites by Coordinated Water Molecules. *Chem. Mater.* **2009**, *21*, 1425–1430.
10. Finsy, V.; Ma, L.; Alaerts, L.; De Vos, D. E.; Baron, G. V.; Denayer, J. F. M. Separation of $CO_2/CH_4$ Mixtures with the MIL-53(Al) Metal-Organic Framework. *Microporous Mesoporous Mater.* **2009**, *120*, 221–227.
11. Dietzel, P. D. C.; Besikiotis, V.; Blom, R. Application of Metal-Organic Frameworks with Coordinatively Unsaturated Metal Sites in Storage and Separation of Methane and Carbon Dioxide. *J. Mater. Chem.* **2009**, *19*, 7362–7370.
12. Babarao, R.; Jiang, J. W. Unprecedentedly High Selective Adsorption of Gas Mixtures in rho Zeolite-Like Metal-Organic Framework: A Molecular Simulation Study. *J. Am. Chem. Soc.* **2009**, *131*, 11417–11425.
13. Demessence, A.; D'Alessandro, D. M.; Foo, M. L.; Long, J. R. Strong $CO_2$ Binding in a Water-Stable, Triazolate-Bridged Metal-Organic Framework Functionalized with Ethylenediamine. *J. Am. Chem. Soc.* **2009**, *131*, 8784–8786.
14. Brtt, D.; Furukawa, H.; Wang, B.; Glover, T. G.; Yaghi, O. M. Highly Efficient Separation of Carbon Dioxide by a Metal-Organic Framework Replete with Open Metal Sites. *Proc. Natl. Acad. Sci. U.S.A.* **2009**, *106*, 20637–20640.
15. Bourrelly, S; Llewellyn, P L; Serre, C; Millange, F.; Loiseau, T.; Férey, G. Different Adsorption Behaviors of Methane and Carbon Dioxide in the Isotypic Nanoporous Metal Terephthalates MIL-53 and MIL-47. *J. Am. Chem. Soc.* **2005**, *127*, 13519–13521.
16. Llewellyn, P. L.; Bourrelly, S.; Serre, C.; Vimont, A.; Daturi, M.; Hamon, L.; De Weireld, G.; Chang, J.-S.; Hong, D.-Y.; Hwang, Y. K.; Jhung, S. H.; Fe'rey, G. High Uptakes of $CO_2$ and $CH_4$ in Mesoporous MetalOrganic Frameworks MIL-100 and MIL-101. *Langmuir* **2008**, *24*, 7245–7250.
17. Banerjee, R.; Phan, A.; Wang, B.; Knobler, C.; Furukawa, H.; O'Keeffe, M.; Yaghi, O. M. High-Throughput Synthesis of Zeolitic Imidazolate Frameworks and Application to $CO_2$ Capture. *Science* **2008**, *319*, 939–943.
18. Cavenati, S.; Grande, C. A.; Rodrigues, A. E. Adsorption Equilibrium of Methane, Carbon Dioxide, and Nitrogen on Zeolite 13X at High Pressures. *J. Chem. Eng. Data* **2004**, *49*, 1095–1101.
19. Wang, B.; Côté, A. P.; Furukawa, H.; O'Keeffe, M.; Yaghi, O. M. Colossal Cages in Zeolitic Imidazolate Frameworks as Selective Carbon Dioxide Reserviors. *Nature* **2008**, *453*, 207–211.
20. Liang, Z. J.; Marshall, M.; Chaffee, A. L. CO2 Adsorption-Based Separation by Metal Organic Framework (Cu-BTC) *versus* Zeolite (13X). *Energy Fuels* **2009**, *23*, 2785–2789.
21. Banerjee, R.; Furukawa, H.; Britt, D.; Knobler, C.; O'Keeffe, M.; M.; Yaghi, O. Control of Pore Size and Functionality in Isoreticular Zeolitic Imidazolate Frameworks and their Carbon Dioxide Selective Capture Properties. *J. Am. Chem. Soc.* **2009**, *131*, 3875–3877.
22. Giovanni, O. D.; Dörfler, W.; Mazzotti, M.; Morbidelli, M. Adsorption of Supercritical Carbon Dioxide on Silica. *Langmuir* **2001**, *17*, 4316–4321.
23. Walton, K. S.; Millward, A. R.; Dubbeldam, D.; Frost, H.; Low, J. J.; Yaghi, O. M.; Snurr, R. Q. Understanding Inflections and Steps in Carbon Dioxide Adsorption Isotherms in Metal-Organic Frameworks. *J. Am. Chem. Soc.* **2008**, *130*, 406–407.
24. Babarao, R.; Jiang, J. Molecular Screening of Metal-Organic Frameworks for $CO_2$ Storage. *Langmuir* **2008**, *24*, 6270–6278.
25. Ramsahye, N. A.; Maurin, G.; Bourrelly, S.; Llewellyn, P. L.; Serre, C.; Loiseau, T.; Devic, T.; Ferey, G. Probing the Adsorption Sites for $CO_2$ in Metal Organic Frameworks Materials MIL-53 (Al, Cr) and MIL-47 (V) by Density Functional Theory. *J. Phys. Chem. C* **2008**, *112*, 514–520.
26. Torrisi, A.; Mellot-Draznieks, C.; Bella, R. G. Impact of Ligands on $CO_2$ Adsorption in Metal-Organic Frameworks: First Principles Study of the Interaction of $CO_2$ with Functionalized Benzenes. I. Inductive Effects on the Aromatic Ring. *J. Chem. Phys.* **2009**, *130*, 194703.
27. Cao, D. P.; Zhang, X. R.; Chen, J. F.; Yun, J.; Wang, W. C. Optimization of Single-Walled Carbon Nanotube Arrays for Methane Storage at Room Temperature. *J. Phys. Chem. B* **2003**, *107*, 13286–13292.
28. Lan, J.; Cheng, D.; Cao, D.; Wang, W. Silicon Nanotubes as a Promising Candidate for Hydrogen Storage: From First-Principle Calculation to GCMC Simulations. *J. Phys. Chem. C* **2008**, *112*, 5598–5604.
29. Cao, D.; Lan, J.; Wang, W.; Smit, B. Li-Doped 3D Covalent Organic Frameworks: High Capacity Hydrogen Storage Materials. *Angew. Chem., Int. Ed.* **2009**, *48*, 4730–4733.
30. Lan, J.; Cao, D.; Wang, W. $Li_{12}Si_{60}H_{60}$ Fullerene Composite: A Promising Hydrogen Storage Medium. *ACS Nano* **2009**, *3*, 3294–3300.
31. Xiang, Z.; Lan, J.; Cao, D.; Shao, X.; Wang, W.; Broom, D. P. Hydrogen Storage in Mesoporous Coordination Frameworks: Experiment and Molecular Simulation. *J. Phys. Chem. C* **2009**, *113*, 15106–15109.
32. Lan, J.; Cao, D. P.; Wang, W. C.; Ben, T.; Zhu, G. S. High Capacity Hydrogen Storage in Porous Aromatic Frameworks with Diamond-Like Structure. *J. Phys. Chem. Lett.* **2010**, *1*, 978–981.
33. Ben, T.; Ren, H.; Ma, S.; Cao, D.; Lan, J.; Jing, X.; Wang, W.; Xu, J.; Deng, F.; Simmons, J. M.; Qiu, S.; Zhu, G. Targeted Synthesis of a Porous Aromatic Framework with High Stability and Exceptionally High Surface Area. *Angew. Chem., Int. Ed.* **2009**, *48*, 9457–9460.
34. Mulfort, K. L.; Hupp, J. T. Chemical Reduction of Metal-Organic Framework Materials as a Method to Enhance Gas Uptake and Binding. *J. Am. Chem. Soc.* **2007**, *129*, 9604–9605.

35. Han, S. S.; Goddard, W. A. III. Lithium-Doped Metal-Organic Frameworks for Reversible $H_2$ Storage at Ambient Temperature. *J. Am. Chem. Soc.* **2007**, *129*, 8422–8423.
36. Mavrandonakis, A.; Tylianakis, E.; Stubos, A. K.; Froudakis, G. E. Why Li Doping in MOFs Enhances $H_2$ Storage Capacity? A Multiscale Theoretical Study. *J. Phys. Chem. C* **2008**, *112*, 7290–7294.
37. Blomqvist, A.; Araújo, C. M.; Srepusharawoot, P.; Ahuja, R. Li-Decorated Metal-Organic Framework 5: A Route to Achieving a Suitable Hydrogen Storage Medium. *Proc. Natl. Acad. Sci. U.S.A.* **2007**, *104*, 20173–20176.
38. Choi, Y. J.; Lee, J. W.; Choi, J. H.; Kang, J. K. Ideal Metal-Decorated Three Dimensional Covalent Organic Frameworks for Reversible Hydrogen Storage. *Appl. Phys. Lett.* **2008**, *92*, 173102.
39. Alapati, S. V.; Johnson, J. K.; Sholl, D. S. Large-Scale Screening of Metal Hydride Mixtures for High-Capacity Hydrogen Storage from First-Principles Calculations. *J. Phys. Chem. C* **2008**, *112*, 5258–5262.
40. Zhou, Z.; Zhao, J.; Chen, Z.; Gao, X.; Yan, T.; Wen, B.; Schleyer, P. V. R. Comparative Study of Hydrogen Adsorption on Carbon and BN Nanotubes. *J. Phys. Chem. B* **2006**, *110*, 13363–13369.
41. Mpourmpakis, G.; Froudakis, G. E.; Lithoxoos, G. P.; Samios, J. SiC Nanotubes: A Novel Material for Hydrogen Storage. *Nano Lett.* **2006**, *6*, 1581–1583.
42. Yildirim, T.; Ciraci, S. Titanium-Decorated Carbon Nanotubes as a Potential High-Capacity Hydrogen Storage Medium. *Phys. Rev. Lett.* **2005**, *94*, 175501.
43. Barman, S.; Sen, P.; Das, G. P. Ti-Decorated Doped Silicon Fullerene: A Possible Hydrogen-Storage Material. *J. Phys. Chem. C* **2008**, *112*, 19963–19968.
44. Yildirim, T.; Iniguez, J.; Ciraci, S. Molecular and Dissociative Adsorption of Multiple Hydrogen Molecules on Transition Metal Decorated C60. *Phys. Rev. B* **2005**, *72*, 153403.
45. Sun, Q.; Wang, Q.; Jena, P.; Kawazoe, Y. Clustering of Ti on a C60 Surface and Its Effect on Hydrogen Storage. *J. Am. Chem. Soc.* **2005**, *127*, 14582–14583.
46. Head-Gordon, M.; Pople, J. A.; Frisch, M. J. MP2 Energy Evaluation by Direct Methods. *Chem. Phys. Lett.* **1988**, *153*, 503–506.
47. Frisch, M. J.; Head-Gordon, M.; Pople, J. A. A Direct MP2 Gradient Method. *Chem. Phys. Lett.* **1990**, *166*, 275–280.
48. Frisch, M. J.; Head-Gordon, M.; Pople, J. A. Semi-Direct Algorithms for the MP2 Energy and Gradient. *Chem. Phys. Lett.* **1990**, *166*, 281–289.
49. Head-Gordon, M.; Head-Gordon, T. Analytic MP2 Frequencies without Fifth-Order Storage: Theory and Application to Bifurcated Hydrogen Bonds in the Water Hexamer. *Chem. Phys. Lett.* **1994**, *220*, 122–128.
50. Frisch, M. J.; Trucks, G. W.; Schlegel, H. B.; Scuseria, G. E.; Robb, M. A.; Cheeseman, J. R. ; Montgomery, J. A., Jr.; Vreven, T.; Kudin, K. N.; Burant, J. C. *Gaussian 03*, revision B.02; Gaussian, Inc.: Wallingford, CT, 2004.
51. Lee, J.-W.; Balathanigaimani, M. S.; Kang, H.-C.; Shim, W.-G.; Kim, C.; Moon, H. Methane Storage on Phenol-Based Activated Carbons at 293.15, 303.15, and 313.15 K. *J. Chem. Eng. Data* **2007**, *52*, 66–70.
52. Becke, A. D. Density Functional Thermochemistry. III. The Role of Exact Exchange. *J. Chem. Phys.* **1993**, *98*, 5648–5652.
53. Feng, X.-B.; Harrison, N. M. Electronic Structure of $CaCuO_2$ from the B3LYP Hybrid Density Functional. *Phys. Rev. B* **2004**, *69*, 132502.
54. Henwood, E.; Carey, J. D. Ab Initio Investigation of Molecular Hydrogen Physisorption on Graphene and Carbon Nanotubes. *Phys. Rev. B* **2007**, *75*, 245413.
55. Lan, J.; Cao, D. P.; Wang, W. C. High Uptakes of Methane in Li-Doped 3D Covalent Organic Frameworks. *Langmuir* **2010**, *26*, 220–226.
56. Tsuzuki, S.; Lüthi, H. P. Interaction Energies of van der Waals and Hydrogen Bonded Systems Calculated Using Density Functional Theory: Assessing the PW91 Model. *J. Chem. Phys.* **2001**, *114*, 3949–3957.
57. Wesolowski, T. A.; Parisel, O.; Ellinger, Y.; Weber, J. Comparative Study of Benzene $\cdots$ X (X = $O_2$, $N_2$, CO) Complexes Using Density Functional Theory: The Importance of an Accurate Exchange-Correlation Energy Density at High Reduced Density Gradients. *J. Phys. Chem. A* **1997**, *101*, 7818–7825.
58. Benco, L.; Demuth, T.; Hafner, J.; Hutschka, F.; Toulhoat, H. Adsorption of Linear Hydrocarbons in Zeolites: A Density-Functional Investigation. *J. Chem. Phys.* **2001**, *114*, 6327–6334.
59. Govind, N.; Andzelm, J.; Reindel, K.; Fitzgerald, G. Zeolite-Catalyzed Hydrocarbon Formation from Methanol: Density Functional Simulations. *Int. J. Mol. Sci.* **2002**, *3*, 423–434.
60. Singh, U. C.; Kollman, P. A. An Approach to Computing Electrostatic Charges for Molecules. *J. Comput. Chem.* **1984**, *5*, 129–145.
61. Besler, B. H.; Merz Jr, K. M.; Kollman, P. A. Atomic Charges Derived From Semiempirical Methods. *J. Comput. Chem.* **1990**, *11*, 431–439.
62. Rappe, A. K.; Goddard, W. A., III. Charge Equilibration for Molecular Dynamics Simulations. *J. Phys. Chem.* **1991**, *95*, 3358–3363.